K.T. KIM[1],✉
C.M. KIM[1]
M.G. BAIK[2]
G. UMESH[1],*
C.H. NAM[1]

Compression of harmonic pulses by using material dispersion

[1] Department of Physics and Coherent X-ray Research Center, Korea Advanced Institute of Science and Technology (KAIST), Daejeon 305-701, Korea
[2] Department of Physics, Kyungwon University, Seongnam, Gyeonggi-do 461-701, Korea

ABSTRACT We utilize the dispersion property of an X-ray filter material for the generation of a single sub-50-as pulse from high-order harmonics. The attosecond pulse, formed by selecting the spectral range of high-order harmonic radiation, contains an intrinsic chirp corresponding to the quadratic phase variation during a half cycle of a laser pulse. We show that this chirp can be compensated by using the negative group-delay dispersion of a thin X-ray filter, compressing the attosecond pulse down to sub-50-as.

PACS 42.65.Re; 42.50.Hz; 42.65.Ky

1 Introduction

The generation of attosecond (as) pulses using high-order harmonic radiation has been an important goal due to its applications. It has been suggested that an attosecond pulse train can be obtained by selecting some harmonics lying in the plateau region by taking advantage of the fact that a regularly spaced harmonic spectrum resembles the spectrum of a mode-locked laser [1]. Attosecond pulses, however, can be produced only if the phase relation between different harmonic orders is favorably set. This theoretical prediction was confirmed in a recent experiment [2, 3]. There have also been suggestions for obtaining a single attosecond pulse [4], which has been confirmed in experiments [5–7]. By selecting the harmonic radiation emitted only near the peak of a femtosecond laser pulse, Kienberger et al. [7] demonstrated the generation of a single attosecond pulse of 250-as duration. According to the studies reported so far on this topic, only a few adjacent harmonics were used for generating the attosecond pulse. This is because the generation of shorter pulses requires a large number of harmonics that can be coherently added. The restriction on the number of selected harmonics is due to the fact that a good phase relationship exists only between adjacent harmonics, unlike the case of the mode-locked laser in which a good phase locking occurs over a wide frequency range. Harmonic radiation emitted with an interval of a half optical cycle normally forms a train of attosecond pulses. The

generation of a single attosecond pulse, on the other hand, requires the use of the harmonic radiation emitted only during a particular half cycle, which is naturally a continuum radiation. The highest frequency of harmonics emitted during each half cycle increases until the pulse peak is reached if the laser intensity is lower than the saturation intensity for optical field ionization. A single attosecond pulse can be produced by selecting the continuum radiation emitted around the pulse peak [5].

There are two crucial requirements to generate such a short pulse – a broad frequency bandwidth and a linear phase relation over the selected frequency range. Although high-order harmonics can support such a broad bandwidth [8, 9], the phase relation between harmonics contains a frequency chirp. In fact, the chirped structure of the harmonics restricts the second requirement, which could seriously limit the resulting pulse duration. Therefore, it is essential to investigate the phase relation between the selected adjacent harmonics in order to obtain the shortest possible pulse duration of either a single attosecond pulse or an attosecond pulse train.

In Sect. 2 we investigate the chirp structure of harmonics and present the results obtained from numerical solutions of the time-dependent Schrödinger equation (TDSE). It is seen that the lack of phase locking between adjacent harmonics mainly arises due to the fact that the high-harmonic signal develops a chirped structure during a half cycle of the laser period. We also calculate an optimum bandwidth for the selection of harmonic radiation to generate the shortest attosecond pulse.

In Sect. 3 a method of how to compensate the chirp is described. We propose to use the dispersion property of an X-ray filter material used for selecting the spectral range of transmitted harmonic radiation. By applying a 5-fs laser pulse on a gas target with an intensity above the saturation intensity for optical field ionization, we obtain a broad continuum radiation from atoms which are subjected to a large nonadiabatic increase of electric field during a half optical cycle. We show from our numerical analysis that a single sub-50-as pulse can be obtained by properly choosing laser parameters and filter material.

2 Chirp structure of harmonics during a half optical cycle

It is well known that high-order harmonics can support a broad bandwidth needed for the generation of a very

✉ Fax: +82-42/869-2510, E-mail: kyungtaec@kaist.ac.kr
*Permanent address: Physics Department, National Institute of Technology Karnataka, Surathkal Mangalore 575025, India

short pulse. Having the bandwidth as broad as possible, however, does not guarantee the shortest pulse when the harmonic radiation is chirped. In order to analyze the chirp structure of the harmonic radiation, we calculated the dipole acceleration by obtaining the numerical solution of the time-dependent Schrödinger equation coupled with Maxwell equations, considering the propagation of an intense femtosecond pulse through gaseous atoms. The effect of focusing and the self-phase modulation due to ionization are incorporated [10]. Figure 1 shows the spectral amplitude of harmonics from neon atoms driven by a 5-fs laser pulse with a peak intensity of $I = 4.7 \times 10^{15}$ W/cm^2. The neon-target medium of 0.5-mm length and of 5-Torr pressure is placed 10 mm behind the laser focus so that only harmonics of short trajectories survive after propagation [11, 12]. Since this intensity is higher than the saturation intensity, all neutral atoms are fully ionized before reaching the peak of the laser pulse envelope. The ionization probability can be estimated by projecting the wave function to the ground state, $1 - \left| \langle \varphi_g | \varphi(t) \rangle \right|^2$, as shown with the laser field in Fig. 2. It is clearly shown that the atoms are fully ionized before $t = -0.5 T_0$. This results in the continuum generation at the high-frequency part of the spectrum. The modulation of harmonics at the lower-frequency region is obvious since the harmonics are generated over several optical cycles. The continuum radiation starts from the frequency of about $100 w_0$ and extends to the cutoff. To understand this spectral structure, one may use the semi-classical theory, which is much simpler than the TDSE.

High-order harmonic generation is well understood in terms of the semi-classical model [13]. An electron tunnels out through the atomic potential well modulated severely by the strong laser field. The ionized electron is accelerated by the intense laser field and it returns to the atomic core when the laser field is reversed in the next half cycle. The kinetic energy of the electron at the time of recombination is released in the form of high-energy photons with frequency

$$\omega(t) = \frac{1}{\hbar} \left(\frac{p(t)^2}{2 m_e} + I_p \right), \tag{1}$$

FIGURE 2 The electric field of the laser pulse (*dashed line*) and the estimated ionization probability (*solid line*) for the case of Fig. 1. The shift of the laser-pulse peak is due to the Gouy phase shift, corresponding to the distance between the laser focus and the medium

where w is the time-dependent carrier frequency, $p(t)$ is the momentum of the electron at the moment of recombination, and I_p is the ionization potential. There are two main paths which contribute to the harmonics – short and long trajectories. When the macroscopic condition is favorably set for the attosecond pulse generation, harmonics are mostly contributed by the short trajectories [11, 12]. The frequency of the short trajectories corresponding to the case of Fig. 1 is shown in Fig. 3. Since harmonic radiation occurs at every half cycle of the laser where the laser intensity is different, the maximum frequency of each half cycle is different, that is $(3.17 U_p(t) + I_p)/\hbar$. The maximum frequency of the curve at $t = -1.5$ in Fig. 3 is about $100 w_0$. The harmonic radiation at $t = -1.0$ generates the continuum radiation as there is no more radiation after that curve because of the depletion of neutral atoms. Consequently, a broad continuum radiation could be generated. Figure 3 explains not only the continuum radiation but also the chirp structure of the harmonic radiation. The harmonics from short trajectories have a positive chirp, as seen from the slopes of the curves in Fig. 3.

We define the chirp coefficient in the time domain as $\alpha = d\omega / dt$. There are two major factors determining the chirp
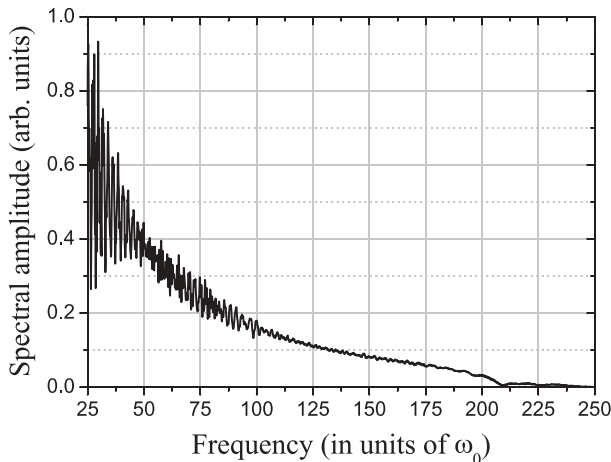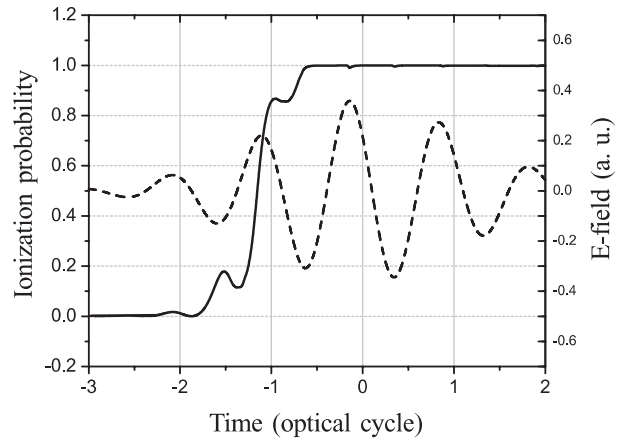
FIGURE 1 Spectral amplitude of high-order harmonic obtained for neon atoms driven by a 5-fs laser pulse with a peak intensity of $I = 4.7 \times 10^{15}$ W/cm^2. The neon-target medium of 0.5-mm length and of 5-Torr pressure is placed 10 mm behind the laser focus
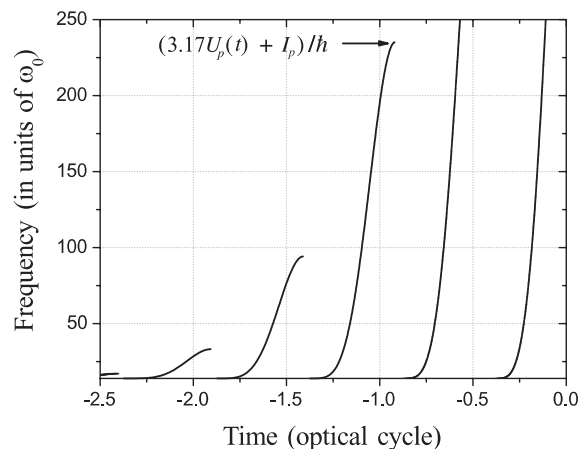
FIGURE 3 Harmonic frequency as given by the semi-classical theory for the conditions of Fig. 1

coefficient. The first factor includes the laser parameters – intensity and frequency. It is shown in Fig. 3 that the highest frequency of each curve is determined by the cutoff rule, $(3.17U_{\mathrm{p}}(t) + I_{\mathrm{p}})/\hbar$. The chirp coefficient is then roughly proportional to U_{p}/T_0 or I/ω_0. Secondly, for each curve the chirp coefficient is larger in a certain bandwidth, as is evident from Fig. 3; it is clear that α has a larger value in the mid-frequency region. Within this frequency bandwidth the chirp coefficient can be approximated as a constant and the corresponding spectral phase $\tilde{\varphi}_{\mathrm{h}}$ can be written as

$$\tilde{\varphi}_{\mathrm{h}}(\omega) = \frac{1}{2\alpha}(\omega - \omega_{\mathrm{c}})^2, \tag{2}$$

where ω_{c} is the center frequency of the bandwidth chosen. To obtain shorter pulses, the variation of the spectral phase should be as small as possible within a desired frequency bandwidth. We can see from (2) that this can be achieved with a large chirp coefficient. Thus, one has to use a high-intensity laser pulse and select a bandwidth in the mid-plateau region. Assuming the use of a Gaussian transmission filter for the frequency selection, the duration of the chirped attosecond pulse, τ, is given by

$$\tau = \frac{4\ln 2}{\Delta\omega}\sqrt{1 + \left(\frac{\Delta\omega^2}{4\alpha\ln 2}\right)^2}. \tag{3}$$

Then, the maximum bandwidth required for minimum pulse width is given by $\Delta\omega = \sqrt{4\alpha\ln(2)}$. Although the generated harmonic bandwidth can be very broad, the maximum usable bandwidth $\Delta\omega_{\max}$ is limited by the existence of the chirp. Thus, the optimized pulse width is proportional to $\sqrt{\omega_0/I}$.

Even though α is so large as to make the phase variation small, the quadratic phase variation can still be large enough to destroy the constructive addition of different frequency components. As the absolute phase and the group delay have no bearing on the pulse width, the quadratic phase in (2) is the most relevant term in determining the temporal profile of an attosecond pulse. Since a much higher laser intensity has no practical importance, we cannot make the quadratic phase variation any smaller. In order to reduce the pulse duration further, it is evident that the chirp of the harmonics must be compensated. The quadratic spectral phase variation, corresponding to the linear chirp, is the same quantity as the group-delay dispersion (GDD) of the material. If there is a material whose GDD is negative while it is transparent in this wavelength region, it can compensate the chirp of the attosecond pulse. Therefore, we need to analyze the dispersion properties of materials, the subject of Sect. 3.

3   Chirp compensation using material dispersion

The refractive index $n(\omega)$ of a material at the frequency ω can be written as

$$n(\omega) = 1 - \delta(\omega) + \mathrm{i}\beta(\omega). \tag{4}$$

Though the imaginary part $\beta(\omega)$ of the refractive index is easily obtained from absorption experiments, the real part $\delta(\omega)$ is not so easy to obtain by a direct measurement. The interferometry for measuring the refractive index of a material is not easy

to implement in the extreme-ultraviolet (XUV) and soft X-ray regions. However the real part of the refractive index can be determined by the Kramers–Kronig relation [14]:

$$\delta(\omega) - \frac{2\pi n_{\mathrm{a}} r_{\mathrm{e}} c^2}{\omega^2} Z = -\frac{2}{\pi\omega^2} P \int\limits_0^\infty \frac{u^3 \beta(u)}{u^2 - \omega^2}\, \mathrm{d}u, \tag{5}$$

where n_{a} is the atomic number density, r_{e} is the classical electron radius, c is the speed of light, and Z is the atomic number. Here P denotes the principal value of the integral.

Figure 4a shows the typical refractive-index curve around an absorption peak. The real part of the refractive index can be divided into three regions – (I) the normal group delay with positive GDD, (II) anomalous group delay, and (III) the normal group delay with negative GDD. The spectral phase shift induced in a material with thickness z can be calculated as

$$\Delta\tilde{\varphi}_{\mathrm{filter}} = -\omega\delta(\omega)z/c, \tag{6}$$

and GDD is the second derivative of this spectral phase shift:

$$\mathrm{GDD} = \frac{\mathrm{d}^2(\Delta\tilde{\varphi}_{\mathrm{filter}})}{\mathrm{d}\omega^2}. \tag{7}$$

It must be noted that the negative GDD region appears just after the absorption peak. Figure 4b shows the real and imaginary values of the refractive index whose absorption is square-well-shaped (corresponding to flat-top transmission). The negative GDD region also appears just after the absorption peak no matter what the shape is – either a single peak (a) or a step (b). This can be explained by looking at the functional form of the Kramers–Kronig relation. Due to the denominator, $u^2 - \omega^2$, in the integral, the major contribution to the real part of the refractive index comes from the region adjacent to ω. Therefore, the behavior of the real part of the refractive
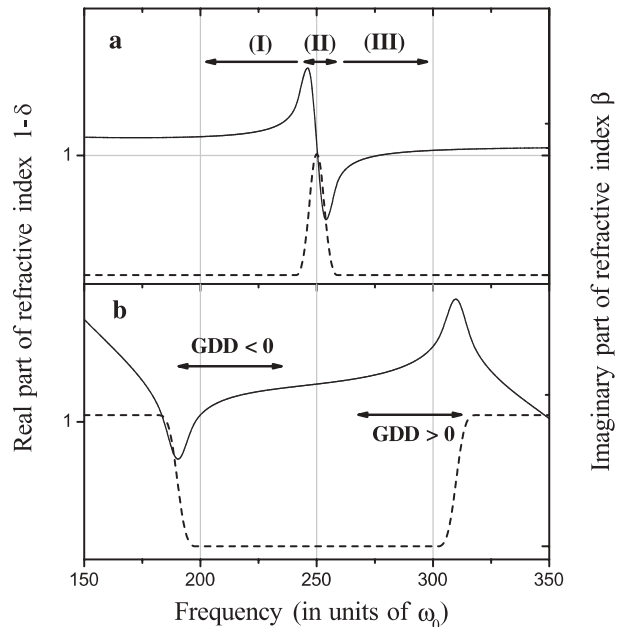

FIGURE 4   Real (*solid line*) and imaginary (*dashed line*) parts of the refractive index for the cases of **a** single-peaked absorption and **b** square-well-shaped absorption

index just after the absorption peak is similar in both cases (a) and (b). Nevertheless, the material with a square-well absorption is suitable due to its bandwidth-selection property. Flat-top transmittance occurs in the frequency region where there is no strong absorption. For example, tin (Sn) has a flat-top transmittance range between M and N absorption edges. There are several materials that have a flat-top-shaped transmission, such as Zr, Ag, In, etc. All these materials are commonly used as X-ray filters and have transmission windows in different frequency regions.

Here we consider two thin filters, Sn and Ti, to check whether their negative GDD values are large enough to compensate the chirp of an attosecond pulse. We can control the GDD by adjusting the thickness of the material, because the GDD is proportional to the thickness of the material. Since the transmittance decays exponentially with increasing filter thickness, material with a small GDD value cannot be used for our purpose. Figure 5a shows the transmittance of 700-nm-thick Sn and Ti, which are commonly used as X-ray filters. Sn has a flat-top transmittance, which we consider to be the ideal case as discussed previously. The GDD values of the two materials are shown in Fig. 5b. The average GDD of Sn between $95\omega_0$ and $135\omega_0$ is $-0.0012\,\mathrm{fs}^2$. Since the chirp coefficient calculated from Fig. 3 is $860\,\mathrm{fs}^{-2}$ and its inverse is $0.0012\,\mathrm{fs}^2$, the Sn filter has a GDD value large enough for compensating the chirp of the harmonics. On the other hand, the transmittance of Ti gradually increases so that the GDD value is not large enough to compensate the chirp of the harmonics in the low-frequency region of the transmission window and the GDD value is positive in the high-frequency region, as can be inferred from Fig. 4. Therefore, we choose the Sn filter for the chirp compensation of the harmonic radiation.
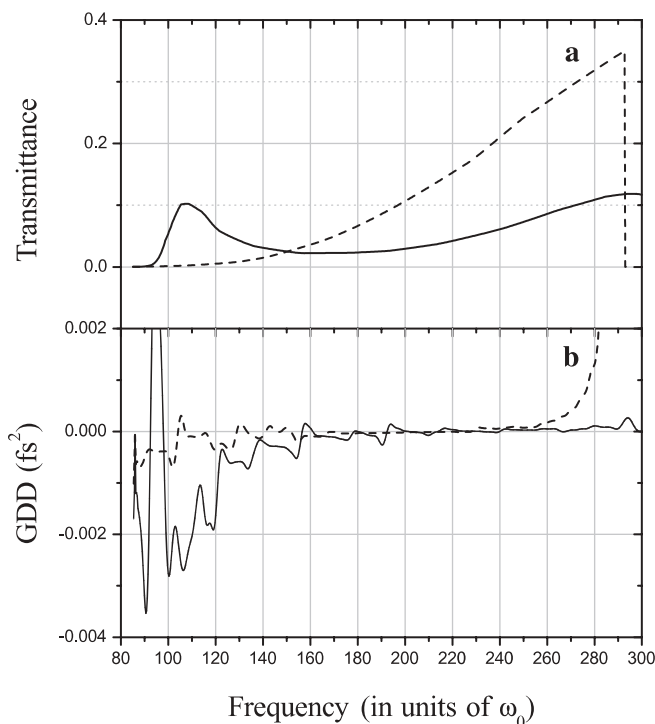

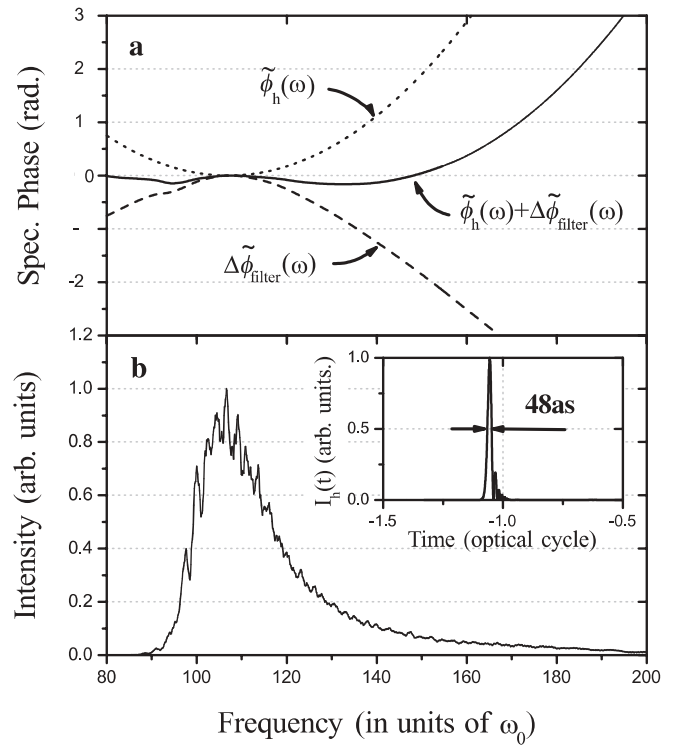**FIGURE 6** **a** Chirp compensation of positively chirped harmonic radiation by a Sn X-ray filter. The spectral phase of the harmonic radiation with a positive linear chirp centered at $107\omega_0$, $\tilde{\varphi}_h(\omega)$, and the spectral phase shift induced by a 700-nm-thick Sn filter, $\Delta\tilde{\varphi}_{\mathrm{filter}}(\omega)$, are shown, respectively, by *dotted* and *dashed lines*. The spectral phase of the harmonic radiation after the Sn filter is shown as the *solid line*. **b** Spectral intensity of the harmonic radiation corresponding to Fig. 1b, transmitted through the 700-nm-thick Sn filter. The *inset* shows the temporal profile of the single 48-as pulse obtained after the Sn filter

The spectral phase of the harmonics $\tilde{\varphi}_h$ calculated using (2) in the case of Fig. 1 is shown as a dotted line in Fig. 6a. The spectral phase shift $\Delta\tilde{\varphi}_{\mathrm{filter}}$ induced by the 700-nm-thick Sn filter material is also shown as a dashed line in Fig. 6a. The spectral phase after passing through the 700-nm-thick Sn filter is the sum of these two. The result is shown by the solid line in Fig. 6a. The spectral phase after passing through the filter material is much less than π over the full width at half maximum of the Sn filter transmittance. This implies that the phase relation is suitable for the coherent addition of the harmonic radiation. The temporal profile of the single attosecond pulse is shown in the inset in Fig. 6b. The pulse duration of the single harmonic pulse is 48 as. It may be compared with the chirp-free Gaussian pulse. The bandwidth of the harmonic spectrum is $26\omega_0$ as shown in Fig. 6b. The width of the chirp-free pulse is 45 as in the case of the Gaussian pulse whose bandwidth is $26\omega_0$. Therefore, the attosecond pulse passing through the suitably chosen filter is almost chirp-free.

4   Conclusion

From the time–frequency analysis of harmonic radiation, we showed that the harmonic radiation has a chirp during a half optical cycle, which seriously affects the shape of the attosecond pulse. We have shown that a 5-fs laser pulse with an intensity above the saturation intensity can generate

FIGURE 5 **a** Transmittance of 700-nm-thick Sn (*solid line*) and Ti (*dashed line*). **b** GDD of 700-nm-thick Sn (*solid line*) and Ti (*dashed line*)

harmonic radiation with a broad continuum. The analysis of the phase relation over the range of the continuum indicates that we may reduce, but not eliminate, the chirp by properly choosing laser parameters. Since materials with negative GDD can compensate the chirp of harmonic radiation, we have chosen an X-ray material with dispersion properties well suited for this purpose. This is done by analyzing the refractive indices of materials obtained using the Kramer–Kronig relation. It turns out that a material with a flat-top transmission window is best suited for chirp compensation. We show that a single 48-as pulse can be generated using this technique.

REFERENCES

1 P. Antoine, A. L'Huillier, M. Lewenstein: Phys. Rev. Lett. **77**, 1234 (1996)
2 P.M. Paul, E.S. Toma, P. Breger, G. Mullot, F. Augé, P. Balcou, H.G. Muller, P. Agostini: Science **292**, 1689 (2001)
3 Y. Mairesse, A. de Bohan, L.J. Frasinski, H. Merdji, L.C. Dinu, P. Monchicourt, P. Breger, M. Kovačev, R. Taïeb, B. Carré, H.G. Muller, P. Agostini, P. Salières: Science **302**, 1540 (2003)
4 I.P. Christov, M.M. Murnane, H.C. Kapteyn: Phys. Rev. Lett. **78**, 1251 (1997)
5 A. Baltuška, T. Udem, M. Uiberacker, M. Hentschel, E. Goulielmakis, C. Gohle, R. Holzwarth, V.S. Yakovlev, A. Scrinzi, T.W. Hänsch, F. Krausz: Nature **421**, 661 (2003)
6 M. Hentschel, R. Kienberger, C. Spielmann, G.A. Reider, N. Milosevic, T. Brabec, P. Corkum, U. Heinzmann, M. Drescher, F. Krausz: Nature **414**, 509 (2001)
7 R. Kienberger, E. Goulielmakis, M. Uiberacker, A. Baltuska, V. Yakovlev, F. Bammer, A. Scrinzi, T. Westerwalbesloh, U. Kleinberg, U. Heinzmann, M. Drescher, F. Krausz: Nature **427**, 817 (2004)
8 Z. Chang, A. Rundquist, H. Wang, M.M. Murnane, H.C. Kapteyn: Phys. Rev. Lett. **79**, 2967 (1997)
9 C. Spielmann, N.H. Burnett, S. Sartania, R. Koppitsch, M. Schnürer, C. Kan, M. Lenzner, P. Wobrauschek, F. Krausz: Science **278**, 661 (1997)
10 J.H. Kim, C.H. Nam: Phys. Rev. A **65**, 033 801 (2002)
11 P. Salières, B. Carré, L. Le Déroff, F. Grasbon, G.G. Paulus, H. Walther, R. Kopold, W. Becker, D.B. Milošević, A. Sanpera, M. Lewenstein: Science **292**, 902 (2001)
12 D.G. Lee, H.J. Shin, Y.H. Cha, K.H. Hong, J.H. Kim, C.H. Nam: Phys. Rev. A **63**, 021 801(R) (2001)
13 P.B. Corkum: Phys. Rev. Lett. **71**, 1994 (1993)
14 B.L. Henke, E.M. Gullikson, J.C. Davis: At. Data Nucl. Data Tables **54**, 181 (1993)